Science Advances
AAAS

advances.sciencemag.org/cgi/content/full/4/11/eaau3488/DC1

Supplementary Materials for

Coalescence-induced jumping of droplets on superomniphobic surfaces with macrotexture

Hamed Vahabi, Wei Wang, Joseph M. Mabry, Arun K. Kota*

*Corresponding author. Email: arun.kota@colostate.edu

Published 9 November 2018, *Sci. Adv.* **4**, eaau3488 (2018)
DOI: 10.1126/sciadv.aau3488

The PDF file includes:

Other Supplementary Material for this manuscript includes the following:

(available at advances.sciencemag.org/cgi/content/full/4/11/eaau3488/DC1)

Movie S1 (.mp4 format). This video illustrates (experimentally and numerically) the coalescence-induced self-propulsion of two droplets of water ($R_0 \approx$ 600 μm) on a superomniphobic surface without a ridge.

Movie S2 (.mp4 format). This video illustrates (experimentally and numerically) the coalescence-induced self-propulsion of two droplets of water ($R_0 \approx 600$ μm) on a superomniphobic surface with a ridge (ridge height $h_r \approx 500$ μm).
Movie S3 (.mp4 format). This video illustrates the evolution of the velocity vectors within two droplets of water ($R_0 \approx 600$ μm) during their coalescence on a superomniphobic surface with and without a ridge.
Movie S4 (.mp4 format). This video illustrates (experimentally and numerically) the coalescence-induced self-propulsion of two droplets ($R_0 \approx 480$ μm) of a low–surface tension liquid (*n*-tetradecane with $\gamma_{lv} \approx 26.6$ mN m^{-1}) on a superomniphobic surface with a ridge.
Movie S5 (.mp4 format). This video illustrates (experimentally and numerically) the coalescence-induced self-propulsion of two droplets ($R_0 \approx 480$ μm) of a high-viscosity liquid (water + 90% glycerol with $\mu \approx 220$ mPa•s) on a superomniphobic surface with a ridge.
Movie S6 (.mp4 format). This video illustrates the coalescence of two low–surface tension droplets (*n*-tetradecane with $\gamma_{lv} \approx 26.6$ mN m^{-1} and $R_0 \approx 480$ μm) and two high-viscosity droplets (water + 90% glycerol with $\mu \approx 220$ mPa•s and $R_0 \approx 480$ μm) on a superomniphobic surface without a ridge.

Supplementary Text

Section S1. Wettability and Morphology of Superomniphobic Surfaces

Table S1. Density, viscosity, surface tension, apparent advancing contact angle, apparent receding contact angle, and roll-off angle of test liquids on superomniphobic surfaces.

Liquid	Density, ρ [kg m^{-3}]	Viscosity, μ [mPa s]	Surface tension, γ_{lv} [mN m^{-1}]	Apparent advancing contact angle, θ^*_{adv} [°]	Apparent receding contact angle, θ^*_{rec} [°]	Roll off angle, ω [°]
Water	998	1	72	171°	164°	3°
water + 90% glycerol	1230	220	64	168°	160°	4°
n-tetradecane	760	2.1	26.6	158°	150°	7°

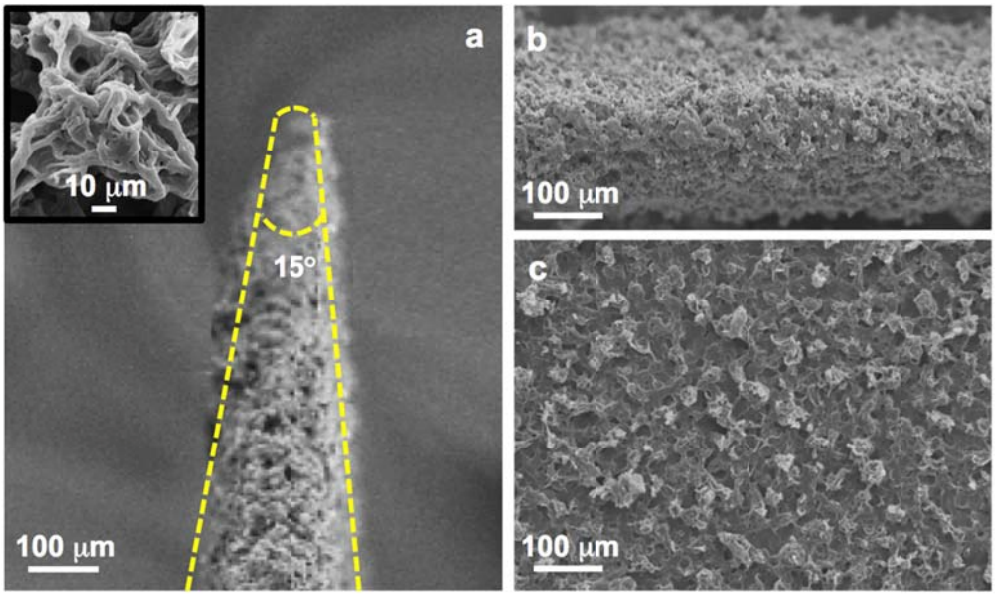

Fig. S1. Morphology of the superomniphobic ridge. (**a**, **b** and **c**) SEM images showing the front view (cross-section), top view and side view, respectively, of the superomniphobic ridge. Inset in (a) shows the texture of the superomniphobic surface.

Section S2. Numerical Domain

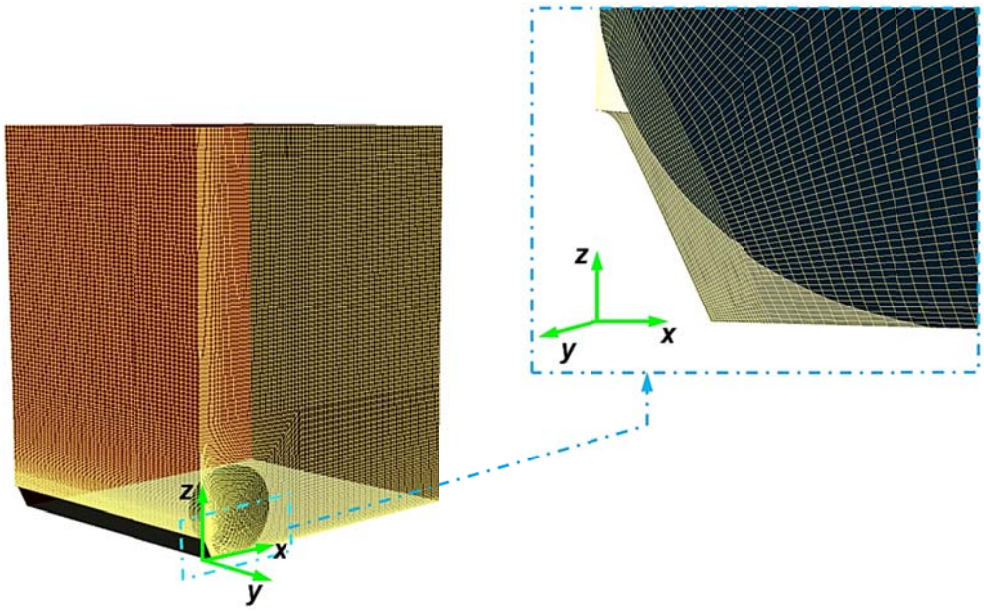

Fig. S2. Computational domain. Half of a coalescing droplet (radius R_0) resting on a superomniphobic surface (at $z = 0$) in a computational domain of volume $6R_0 \times 6R_0 \times 10R_0$. Finer mesh (inset) was used close to the ridge, the lower boundary of the computational domain (i.e., $z \rightarrow 0$) and also close to the symmetric planes (i.e., $x \rightarrow 0$ and $y \rightarrow 0$) to mitigate the influence of high gradients.

Section S3. Components of Velocity

The volume of fluid (VOF) model is employed here to simulate the two immiscible fluids (i.e., air *a* and the test liquid *l*) by solving a single set of momentum equations and tracking the volume fraction of each of the phases throughout the domain.(*39*) This model assumes that each cell within the computational domain contains either one phase (i.e., air *a* or test liquid *l*) or two phases (i.e., both air *a* or test liquid *l*) separated by an interface. In each cell, the volume fraction β of each phase is tracked. For example, if the cell contains only the test liquid, $\beta_l = 1$ and $\beta_a = 0$; and when the cell contains both the phases, $0 < \beta_l < 1$ and $0 < \beta_a < 1$. For each cell, equivalent properties (e.g., density ρ) of the phase mixture are calculated by a rule of mixtures as $\rho_{cell,eq} = \beta_{cell,a}\rho_a + \beta_{cell,l}\rho_l$, where $\beta_{cell,l} + \beta_{cell,a} = 1$. The mass of each cell is $m_{cell} = \rho_{cell,eq}\phi_{cell}$, where ϕ_{cell} is the volume of the cell. The equivalent properties are then used to solve a single set of momentum equations at each cell throughout the computational domain and determine the velocity components for each cell (i.e., $V_{cell,x}$, $V_{cell,y}$ and $V_{cell,z}$). At each time step, once the volume fractions $\beta_{cell,a}$(t) and $\beta_{cell,l}$(t) and the velocity components $V_{cell,x}$(t), $V_{cell,y}$(t) and $V_{cell,z}$(t) are determined for each cell, the magnitude of velocity for each cell is determined as

$$V_{cell,total}(t) = \left\{V_{cell,x}^2(t) + V_{cell,y}^2(t) + V_{cell,z}^2(t)\right\}^{1/2} \quad \text{(S1)}$$

During coalescence, the droplet deforms symmetrically relative to the *xz* and *yz* planes (see fig. S2). Consequently, at each time step, the net velocity of the droplet in x direction $V_{net,x}$(t) = 0 and the net velocity of the droplet in the y direction $V_{net,y}$(t) = 0 (i.e., the center of mass of the droplet does not move in the *x* direction or the *y* direction). However, due to symmetry breaking caused

by the superomniphobic surface without or with a ridge, the net velocity of the droplet in z direction (i.e., net upward velocity of the droplet) $V_{net,z}(t) = V_{up}(t) \neq 0$. Recognizing that different cells in the computational domain have different mass, this net upward velocity can be estimated through the mass-weighted average of the z component of the velocity in each cell as

$$V_{up}(t) = \frac{\sum \left\{ m_{cell,+z}(t)\, V_{cell,+z}(t) - m_{cell,-z}(t)\, V_{cell,-z}(t) \right\}}{m_c} \tag{S2}$$

Here, $m_{cell,+z}$(t) and $V_{cell,+z}$(t) are the mass and the magnitude of the z component of the velocity in cells with positive (i.e., upward) $V_{cell,z}$(t). Similarly, $m_{cell,-z}$(t) and $V_{cell,-z}$(t) are the mass and the magnitude of the z component of the velocity in cells with negative (i.e., downward) $V_{cell,z}$(t).

Note that $m_c = \rho 4\pi R_c^3 / 3$ is the mass of the coalesced droplet.

Section S4. In-plane, Out-of-plane and Total Kinetic Energy

During coalescence, the excess surface energy $E_{surf,ex}(t)$ of the droplet is released (see Fig. 2a and 3a) and partly converted into the total kinetic energy $E_{kin,total}(t)$ of the droplet. The total kinetic energy of the droplet can be estimated as the sum of the total kinetic energy of the cells within the entire computational domain as

$$E_{kin,total}(t) = \frac{1}{2}\sum\left\{m_{cell}(t)V_{cell,total}^2(t)\right\} \tag{S3}$$

Note that $V_{cell,total}(t)$ is defined by equation S1 and the total kinetic energy $E_{kin,total}(t)$ of the droplet is the sum of the in-plane kinetic energy (in *x* and *y* directions) and out-of-plane kinetic energy (in the *z* direction). During the coalescence, the in-plane kinetic energy manifests as symmetric deformation of the droplet (relative to the *xz* and *yz* planes), in the plane of coalescence (i.e., *xy* plane, see Fig. 2b through 2f, Fig.3b through 3f and Section S5). During stage I of coalescence (see Fig. 2a and 3a), the out-of-plane kinetic energy manifests as symmetric deformation of the droplet perpendicular to the plane of coalescence. During stages II and III of coalescence (see Fig. 2a and 3a), the out-of-plane kinetic energy manifests as both the deformation of the droplet perpendicular to the plane of coalescence and net motion of the center of mass of the droplet in the upward (i.e., +*z*) direction (see Fig. 2c through 2f and Fig. 3c through 3f as well as Section S5). The upward kinetic energy (i.e., kinetic energy by virtue of the net upward velocity) is a fraction of the total kinetic energy of the droplet that is given as

$$E_{kin,up}(t) = \frac{1}{2}m_c V_{up}^2(t) \tag{S4}$$

V_{up}(t) is defined by equation S2. In our analysis, we non-dimensionalized the total kinetic energy as $E^*_{kin,total}(t^*) = E_{kin,total}(t) \big/ E_{surf,ex}(0)$, and the upward kinetic energy as $E^*_{kin,up}(t^*) = E_{kin,up}(t) \big/ E_{surf,ex}(0)$. Comparison of the kinetic energies of a coalescing water droplet (R_0 = 600 μm) on a superomniphobic surface with a ridge (ridge height $h_r \approx$ 500 μm) and without a ridge (see fig. S3a and S3b) indicates that the ratio of the upward kinetic energy to the total kinetic energy when the droplet departs from the surface $E^*_{kin,up}(t^*_d) \big/ E^*_{kin,total}(t^*_d) \approx$ 76% and 19% for with and without a ridge, respectively. This implies a more effective redirection of velocity vectors during coalescence on a superomniphobic surface with a ridge compared to that on a superomniphobic surface without a ridge.

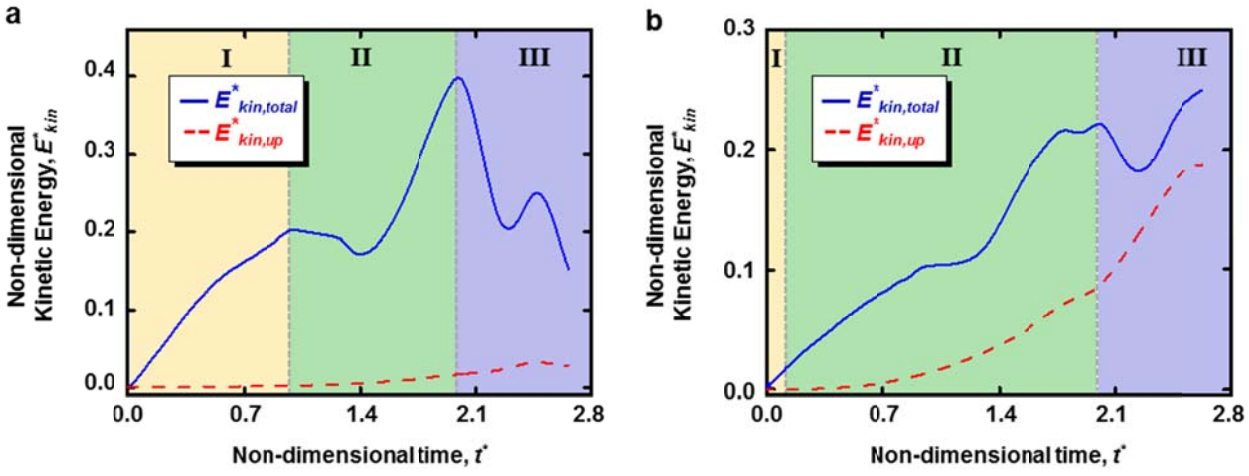

Fig. S3. Components of the total kinetic energy. Evolution of the non-dimensional total kinetic energy $E^*_{kin,total}$ and the upward kinetic energy of the droplets $E^*_{kin,up}$ coalescing on a superomniphobic surface **a)** without and **b)** with a ridge.

Section S5. Evolution of the Droplet Dynamics (*yz* view) during Droplet Coalescence

Evolution of droplet dynamics (pressure field and velocity vectors) during coalescence on a superomniphobic surface without and with a ridge is shown in Figs. 2 and 3 (*xz* view) and fig. S4 (*yz* view).

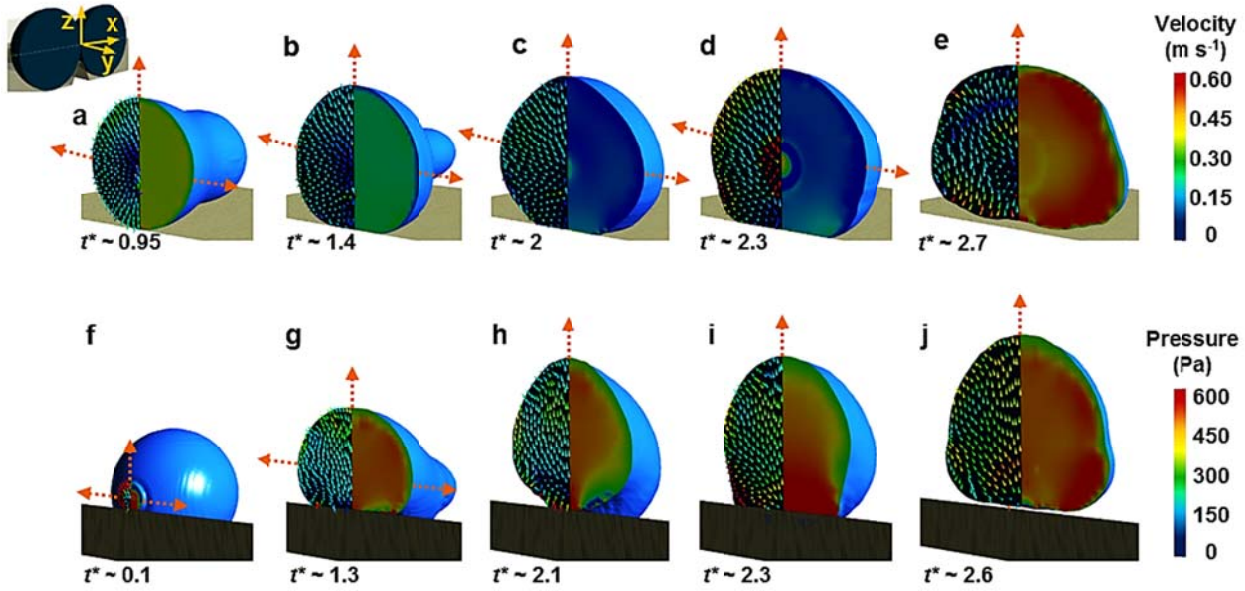

Fig. S4. Velocity vectors and pressure distribution (*yz* view). (**a**-**e**) A series of snapshots showing the pressure distribution and velocity vectors within the droplet on a superomniphobic surface without a ridge; (**f**-**j**) A series of snapshots showing the pressure distribution and velocity vectors within the droplet on a superomniphobic surface with a ridge (ridge height $h_r \approx 500$ μm). The colors represent the magnitude of pressure and velocity. Also see Movie S3.

Section S6. Applicability to Smaller Droplets (R_0 < 10 μm)

We demonstrated that our strategy to enhance the energy conversion efficiency in coalescence-induced jumping of droplets by using a ridge (with height comparable to the droplet radius) is applicable to droplets with radius R_0 on the order of tens of μm to hundreds of μm (see Fig. 4 in the manuscript). In some applications (e.g., condensation), there can be a wide droplet size distribution, including smaller droplets with radius R_0 < 10 μm. In order to demonstrate that our strategy can indeed be applied to smaller droplets with radius R_0 < 10 μm, we conducted numerical simulations on coalescence of water droplets with R_0 = 5 μm on superomniphobic surfaces (water contact angle θ = 165°) without a ridge and with a ridge (non-dimensional ridge height h^* = 0.95, i.e., ridge height h_r ~ 4.75 μm). Our results (see fig. S5) indicate that on the superomniphobic surface without a ridge the energy conversion efficiency $\eta \approx 1.8\%$ (coalesced droplet can barely jump away), while on the superomniphobic surface with a ridge, the energy conversion efficiency $\eta \approx 22.3\%$ (i.e., about 1200% increase in energy conversion efficiency).

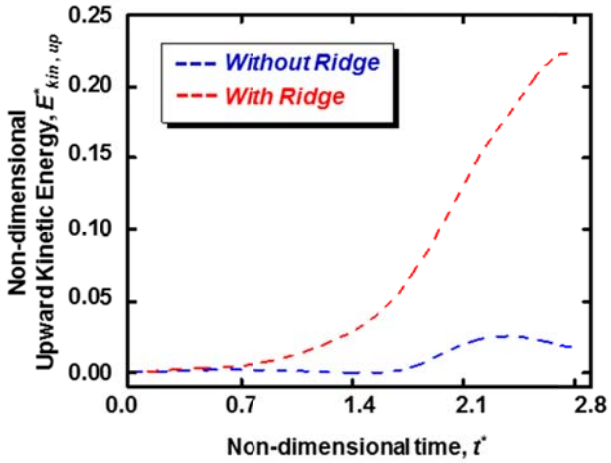

Fig. S5. Coalescence-induced jumping of smaller droplets. Evolution of the non-dimensional upward kinetic energy ($E^*_{kin,up}$) during the coalescence of water droplets ($R_0 \approx 5$ μm) on a superomniphobic surface without and with a ridge (h^* = 0.95).

Section S7. Coalescence of Low Surface Tension and High Viscosity Droplets

Coalescence of low surface tension droplets (e.g., n-tetradecane with $\mu \approx 2.1$ mPa s, $\rho \approx 760$ kg m^{-3}, $\gamma_{lv} \approx 26.6$ mN m^{-1}, $R_0 \approx 480$ μm) and high viscosity droplets (e.g., water + 90% glycerol(*31*) with $\mu \approx 220$ mPa s, $\rho \approx 1230$ kg m^{-3}, $\gamma_{lv} \approx 64$ mN m^{-1}, $R_0 \approx 480$ μm) on superomniphobic surfaces without a ridge is shown in fig. S6a and S6b, respectively (also see **Movie S6**). It is evident that the low surface tension and high viscosity droplets cannot jump away from a superomniphobic surface without a ridge.

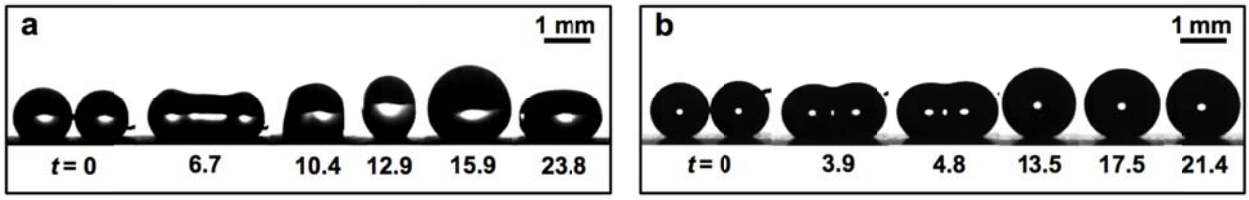

Fig. S6. Coalescence of low–surface tension and high-viscosity droplets. (**a**) A series of snapshots showing the coalescence of n-tetradecane droplets on a superomniphobic surface without a ridge. (**b**) A series of snapshots showing the coalescence of water + 90% glycerol droplets on a superomniphobic surface without a ridge. Note the droplets cannot jump away from the surfaces. Also see Movie S6.

Section S8. Relationship between η and We_j

When a coalesced droplet departs from a super-repellent surface at $t = t_d$ (i.e., at $t^* = t_d^*$), the energy conversion efficiency is defined as

$$\eta = E_{kin,up}(t_d) \Big/ E_{surf,ex}(0) = E_{kin,up}^*(t_d^*) \tag{S5}$$

Here, $E_{kin,up}(t_d) = m_c V_j^2 \Big/ 2$ is the upward kinetic energy, $m_c = \rho \frac{4}{3} \pi R_c^3$ is the mass of the coalesced droplet, V_j is the jumping velocity of the coalesced droplet ($V_j = V_{up}(t_d)$), and

$E_{surf,ex}(0) = E_{surf}(0) - E_{surf,c}$ is the total available excess surface energy, where

$E_{surf}(0) = \gamma_{lv} 8\pi R_0^2$ is the surface energy of droplets at the onset of coalescence and

$E_{surf,c} = \gamma_{lv} 4\pi R_c^2$ is the surface energy of the coalesced droplet that has eventually attained the radius R_c. Recognizing that $R_c = 2^{1/3} R_0$, equation S5 can be rewritten in terms of the Weber number We_j at $t = t_d$ as

$$\eta = \frac{E_{kin,up}(t_d)}{E_{surf,ex}(0)} = \frac{\rho \frac{4}{3} \pi R_c^3 V_j^2 \Big/ 2}{\gamma_{lv} 8\pi R_0^2 - \gamma_{lv} 4\pi R_c^2} \approx 0.8 \frac{\rho R_0 V_j^2}{\gamma_{lv}} \approx 0.8 We_j \tag{S6}$$

Section S9. Hierarchical Structure for Coalescence-induced Jumping of Droplets at Different Length Scales

Our results indicate that super-repellent surfaces designed with macrotextures (e.g., triangular ridges with height comparable to the droplet radius) can enhance the energy conversion efficiency in coalescence-induced jumping of droplets. This can have significant implications for a wide variety of applications including self-cleaning, anti-icing, energy harvesting, hot spot cooling, lab-on-chip devices and condensation, especially with high viscosity and/or low surface tension droplets.

If the enhanced energy conversion efficiency is to be obtained throughout the super-repellent surface, it requires a periodic arrangement of triangular ridges (e.g., discrete tetrahedrons or continuous ridges) with height comparable to the droplet radius. In some applications (e.g., condensation), there can be a wide droplet size distribution, spreading over multiple length scales. If the enhanced energy conversion efficiency is to be obtained in such cases, it requires a super-repellent surface that is hierarchically structured with ridges at multiple length scales so that the finer ridges can enhance the energy conversion efficiency for the smaller droplets and the coarser ridges can enhance the energy conversion efficiency for the larger droplets (see fig. S7a). On such surfaces, at each ridge of each length scale, we anticipate heterogeneous nucleation to predominantly occur along the edges of the base of the ridge due to lower free energy barrier (*34, 35*), followed by droplet growth and coalescence-induced jumping with enhanced energy conversion efficiency (Fig. S7b). Further, for each application, the geometry, size and pitch of the ridges at each length scale must be optimized within the parametric space allowed by the fabrication techniques and the geometric limitations for coalescence – ridge angle $\alpha < \alpha_{max}$ (see supplementary text section S10) and the ridge height $h_r \leq D$ (half the inter-feature spacing).

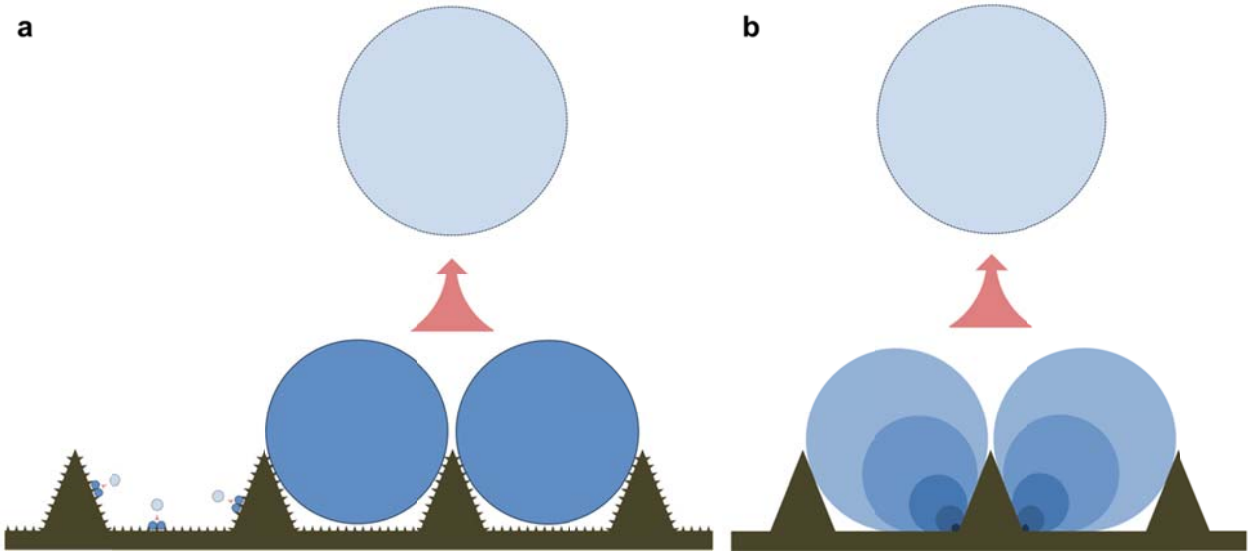

Fig. S7. Schematic of a superrepellent surface with periodic arrangement of triangular ridges. (**a**) Super-repellent surfaces with hierarchically structured ridges at two length scales. The finer ridges enhance the energy conversion efficiency for the smaller droplets and the coarser ridges enhance the energy conversion efficiency for the larger droplets. (**b**) Heterogeneous nucleation (along the edges of the base of the ridge) and droplet growth, followed by coalescence-induced jumping on the super-repellent ridge.

Section S10. Influence of the Ridge Angle

Prior to investigating the influence of the ridge angle α on the energy conversion efficiency η, it is important to recognize that there is a geometric limitation on the ridge angle α for coalescence to occur. For a ridge height h_r and droplet radius R_0 (i.e., non-dimensional ridge height, $h^* = h_r / R_0$), there is a maximum ridge angle α_{max} beyond which coalescence cannot occur because the ridge physically obstructs the droplets from contacting each other.

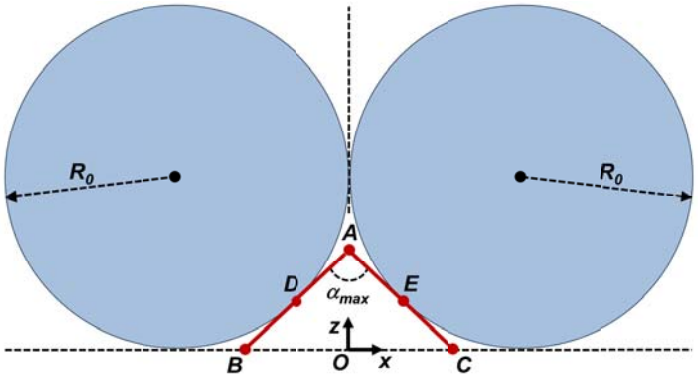

Fig. S8. Schematic of two coalescing droplets and a ridge with maximum ridge angle.

In order to determine α_{max}, consider a 2D view of the *xz* plane (fig. S8; *y*-axis is into and out of the plane of the figure) with two identical droplets of radius R_0 contacting each other, just prior to coalescing symmetrically relative to the *yz* plane. Now, consider a triangular ridge (*ABC* in fig. S8) of height $OA = h_r$, located symmetrically relative to the *yz* plane, between the two coalescing droplets, with the maximum possible ridge angle $BAC = \alpha_{max}$. When the ridge angle $\alpha > \alpha_{max}$, the ridge physically obstructs the droplets from contacting each other, thereby preventing coalescence. When $\alpha = \alpha_{max}$, each ridge arm (*AB* and *AC*) contacts each droplet tangentially (at *D* and *E*). Say, the origin is at *O*, then the ridge peak *A* is $(0, h_r)$. Let the tangential contact point *E* be (x_E, y_E). The slope *m* of the tangent *AEC* to the circle (representing the right droplet), is given as

$$m = -\frac{x_E - R_0}{z_E - R_0} \tag{S7}$$

The slope m of the line AE in terms of the ridge height h_r, is given as

$$m = -\frac{h_r - z_E}{x_E} \tag{S8}$$

Combining equations S7 and S8 and recognizing that $E(x_E, y_E)$ must satisfy the equation of the circle (representing the right droplet), $(x - R_0)^2 + (z - R_0)^2 = R_0^2$, we obtain

$$x_E = \frac{2R_0(R_0 - h_r)^2}{R_0^2 + (R_0 - h_r)^2} \;\&\; z_E = \frac{R_0 h_r^2}{R_0^2 + (R_0 - h_r)^2} \tag{S9}$$

Now, recognizing that $\tan\left(\frac{\alpha_{max}}{2}\right) = \frac{x_E}{h_r - z_E}$, and using equation S9, we obtain

$$\alpha_{max} = 2\tan^{-1}\left\{\frac{2(1-h^*)}{1-(1-h^*)^2}\right\} \tag{S10}$$

It is evident from equation S10 that as $h^* \to 0$ (i.e., when the ridge height is negligible compared to the droplet radius), $\alpha_{max} \to \pi$; and as $h^* \to 1$ (i.e., when the ridge height approaches the droplet radius), $\alpha_{max} \to 0$. As may be anticipated, physically, it implies that as the ridge height

increases, the ridge should be sharper (i.e., the maximum ridge angle is smaller) to prevent physical obstruction and allow coalescence, i.e., as h^* increases, α_{max} decreases (see fig. S9).

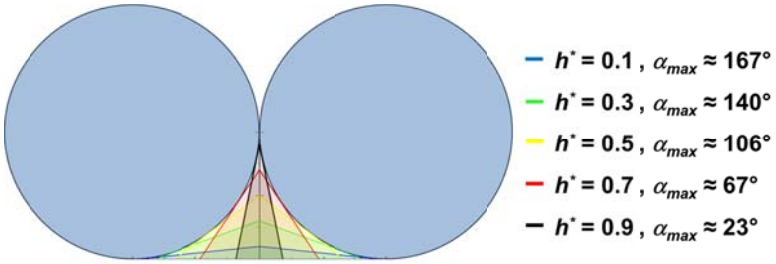

Fig. S9. Schematic depicting the influence of nondimensional ridge height *h on the maximum ridge angle α_{max}.**

In order to determine if the ridge angle α influences the energy conversion efficiency η significantly, we conducted numerical simulations at a low ridge angle ($\alpha \approx 10°$) and a high ridge angle ($\alpha \to \alpha_{max}$) for non-dimensional ridge heights $h^* = 0.1, 0.5, 0.9$. Our results (see **Table S2**) indicate that η increases with increasing α (especially evident at lower h^*). This is because, as α increases, the ridge intervenes in the coalescence process earlier and leads to effective redirection of in-plane velocity vectors to out-of-plane. From a fundamental standpoint, a more detailed study is necessary to thoroughly understand the influence of the ridge angle α on the detailed droplet dynamics. From an applied standpoint, the increase in energy conversion efficiency η due to increase in ridge angle α is limited to lower non-dimensional ridge heights h^* (with lower energy conversion efficiency η); and it is not as significant as the increase in energy conversion efficiency η due to increase in non-dimensional ridge height h^*.

Table S2. Influence of the ridge angle α on the energy conversion efficiency η in coalescence-induced jumping of droplets with radius R_0 = 600 μm at different nondimensional ridge heights h^*.

h^*	α [°]	η [%]
0.1	10	4.9
0.1	160	8.0
0.5	10	11.8
0.5	100	13.5
0.9	10	18.8
0.9	20	18.9

Movie Legends

Movie S1. This video illustrates (experimentally and numerically) the coalescence-induced self-propulsion of two droplets of water ($R_0 \approx 600$ μm) on a superomniphobic surface without a ridge. The fiber visible in the movie is the maneuvering probe.

Movie S2. This video illustrates (experimentally and numerically) the coalescence-induced self-propulsion of two droplets of water ($R_0 \approx 600$ μm) on a superomniphobic surface with a ridge (ridge height $h_r \approx 500$ μm). The fiber visible in the movie is the maneuvering probe.

Movie S3. This video illustrates the evolution of the velocity vectors within two droplets of water ($R_0 \approx 600$ μm) during their coalescence on a superomniphobic surface with and without a ridge. Colors of the velocity vectors represent the velocity magnitude and the legends represent the range of velocity magnitude shown with different colors. Further, evolution of the non-dimensional excess surface energy $E^*_{surf,ex}$ and also the non-dimensional upward kinetic energy $E^*_{kin,up}$ of the droplets during the coalescence on a superomniphobic surface with and without a ridge is shown.

Movie S4. This video illustrates (experimentally and numerically) the coalescence-induced self-propulsion of two droplets ($R_0 \approx 480$ μm) of a low–surface tension liquid (*n*-tetradecane with $\gamma_{lv} \approx 26.6$ mN m^{-1}) on a superomniphobic surface with a ridge. The fiber visible in the movie is the maneuvering probe.

Movie S5. This video illustrates (experimentally and numerically) the coalescence-induced self-propulsion of two droplets ($R_0 \approx 480$ μm) of a high-viscosity liquid (water + 90% glycerol with $\mu \approx 220$ mPa•s) on a superomniphobic surface with a ridge. The fiber visible in the movie is the maneuvering probe.

Movie S6. This video illustrates the coalescence of two low–surface tension droplets (*n*-tetradecane with $\gamma_{lv} \approx 26.6$ mN m^{-1} and $R_0 \approx 480$ μm) and two high-viscosity droplets (water + 90% glycerol with $\mu \approx 220$ mPa•s and $R_0 \approx 480$ μm) on a superomniphobic surface

without a ridge. The coalesced droplet cannot jump away from the superomniphobic surface without a ridge. The fiber visible in the movie is the maneuvering probe.